A Modified Fuzzy C-Means Algorithm for Bias Field Estimation and Segmentation of MRI Data

Mohamed N. Ahmed, *Member, IEEE*, Sameh M. Yamany, *Member, IEEE*, Nevin Mohamed, Aly A. Farag*, *Senior Member, IEEE*, and Thomas Moriarty

***Abstract*—In this paper, we present a novel algorithm for fuzzy segmentation of magnetic resonance imaging (MRI) data and estimation of intensity inhomogeneities using fuzzy logic. MRI intensity inhomogeneities can be attributed to imperfections in the radio-frequency coils or to problems associated with the acquisition sequences. The result is a slowly varying shading artifact over the image that can produce errors with conventional intensity-based classification. Our algorithm is formulated by modifying the objective function of the standard fuzzy c-means (FCM) algorithm to compensate for such inhomogeneities and to allow the labeling of a pixel (voxel) to be influenced by the labels in its immediate neighborhood. The neighborhood effect acts as a regularizer and biases the solution toward piecewise-homogeneous labelings. Such a regularization is useful in segmenting scans corrupted by salt and pepper noise. Experimental results on both synthetic images and MR data are given to demonstrate the effectiveness and efficiency of the proposed algorithm.**

***Index Terms*—Bias field, fuzzy logic, image segmentation, MR imaging.**

I. Introduction

SPATIAL intensity inhomogeneity induced by the radio-frequency coil in magnetic resonance imaging (MRI) is a major problem in the computer analysis of MRI data [1]–[4]. Such inhomogeneities have rendered conventional intensity-based classification of MR images very difficult, even with advanced techniques such as nonparametric, multichannel methods [5]–[7]. This is due to the fact that the intensity inhomogeneities appearing in MR images produce spatial changes in tissue statistics, i.e., mean and variance. In addition, the degradation on the images obstructs the physician's diagnoses because the physician has to ignore the inhomogeneity artifact in the corrupted images [8].

The removal of the spatial intensity inhomogeneity from MR images is difficult because the inhomogeneities could change with different MRI acquisition parameters from patient to patient and from slice to slice. Therefore, the correction of intensity inhomogeneities is usually required for each new image. In the last decade, a number of algorithms have been proposed for the intensity inhomogeneity correction. Meyer *et al.* [9] presented an edge-based segmentation scheme to find uniform regions in the image followed by a polynomial surface fit to those regions. The result of their correction is, however, very dependant on the quality of the segmentation step.

Several authors have reported methods based on the use of phantoms for intensity calibration. Wicks *et al.* [3] proposed methods based on the signal produced by a uniform phantom to correct for MRI images of any orientation. Similarly, Tincher *et al.* [10] modeled the inhomogeneity function by a second-order polynomial and fitted it to a uniform phantom-scanned MR image. These phantom approaches, however, have the drawback that the geometry relationship of the coils and the image data is typically not available with the image data. They also require the same acquisition parameters for the phantom scan and the patient. In addition, these approaches assume the intensity corruption effects are the same for different patients, which is not valid in general [8].

The homomorphic filtering approach to remove the multiplicative effect of the inhomogeneity has been commonly used due to its easy and efficient implementation [6], [11]. This method, however, is effective only on images with relatively low-contrast. Some researchers [10], [12] reported undesirable artifacts with this approach.

Dawant *et al.* [12] used operator-selected reference points in the image to guide the construction of a thin-plate spline correction surface. The performance of this method depends substantially on the labeling of the reference points. Considerable user interactions are usually required to obtain good correction results. More recently, Gilles *et al.* [13] proposed an automatic and iterative B-spline fitting algorithm for the intensity inhomogeneity correction of breast MR images. The application of this algorithm is restricted to MR images with a single dominant tissue class, such as breast MR images. Another polynomial surface fitting method [14] was proposed based on the assumption that the number of tissue classes, the true means, and standard deviations of all the tissue classes in the image are given. Unfortunately, the required statistical information is usually not available.

A different approach used to segment images with intensity inhomogeneities is to simultaneously compensate for the shading effect while segmenting the image. This approach has the advantage of being able to use intermediate information

Manuscript received March 2, 2000; revised January 11, 2002. This work was supported in part by the Norton Health Care System under Grant 97-33 and Grant 97-72) and in part by the National Institutes of Health (NIH) under Grant USHS CA79178-01. The work of T. Moriarty was supported by the Whitaker Foundation under Research Grant RG-98-009. The Associate Editor responsible for coordinating the review of this paper and recommending its publication was L. Clarke. *Asterisk indicates corresponding author*.

M. N. Ahmed and S. M. Yamany are with the Systems and Biomedical Engineering Department, Cairo University, Giza, Egypt

N. Mohamed is with Trendium Corporation, Weston, FL 33326 USA.

*A. A. Farag is with the Computer Vision and Image Processing Laboratory, Department of Electrical and Computer Engineering, Room 415, University of Louisville, Louisville, KY 40292 USA (e-mail: farag@cairo.spd.louisville.edu).

T. Moriarty is with the Department of Neurological Surgery, University of Louisville, Louisville, KY 40292 USA.

Publisher Item Identifier S 0278-0062(02)04088-0.

from the segmentation while performing the correction. Recently, Wells *et al.* [5] developed a new statistical approach based on the expectation-maximization (EM) algorithm to solve the bias-field-correction problem and the tissue classification problem. Guillemaud and Brady [15] further refined this technique by introducing the extra class "other." There are two main disadvantages of this EM approach. First, the EM algorithm is extremely computationally intensive, especially for large problems. Second, the EM algorithm requires a good initial guess for either the bias field or for the classification estimate. Otherwise, the EM algorithm could be easily trapped in a local minimum, resulting in an unsatisfactory solution [8].

Another approach based on the fuzzy c-means (FCM) [17], [18] clustering technique was introduced lately [19]–[21]. FCM has been used with some success in image segmentation in general [22], [23] and also in segmenting MR images [24]–[27]. Xu *et al.* [19] proposed a new adaptive FCM technique to produce fuzzy segmentation while compensating for intensity inhomogeneities. Their method, however, is also computationally intensive. They reduced the computational complexity by iterating on a coarse grid rather the fine grid containing the image. This introduced some errors in the classification results and was found to be sensitive to a considerable amount of salt and pepper noise [20].

To solve the problem of noise sensitivity and computational complexity of Pham and Prince method, we present in this paper a different approach for fuzzy segmentation of MRI data in the presence of intensity inhomogeneities. Our novel algorithm is formulated by modifying the objective function of the standard FCM algorithm to compensate for such inhomogeneities. This new formulation allows the labeling of a pixel (voxel) to be influenced by the labels in its immediate neighborhood. The neighborhood effect acts as a regularizer and biases the solution toward piecewise-homogeneous labeling; such a regularization is useful in segmenting scans corrupted by salt and pepper noise.

II. Background

The observed MRI signal is modeled as a product of the true signal generated by the underlying anatomy, and a spatially varying factor called the gain field

$$Y_k = X_k G_k \qquad \forall\, k \in \{1, 2, \ldots, N\} \tag{1}$$

where X_k and Y_k are the true and observed intensities at the kth voxel, respectively, G_k is the gain field at the kth voxel, and N is the total number of voxels in the MRI volume.

The application of a logarithmic transformation to the intensities allows the artifact to be modeled as an additive bias field [5]

$$y_k = x_k + \beta_k \qquad \forall\, k \in \{1, 2, \ldots, N\} \tag{2}$$

where x_k and y_k are the true and observed log-transformed intensities at the kth voxel, respectively, and β_k is the bias field at the kth voxel. If the gain field is known, then it is relatively easy to estimate the tissue class by applying a conventional intensity-based segmenter to the corrected data. Similarly, if the tissue classes are known, then we can estimate the gain field, but it may be problematic to estimate either without the knowledge of the other. We will show that by using an iterative algorithm based on fuzzy logic, we can estimate both.

III. Bias-Corrected (BC) FCM (BCFCM) Objective Function

The standard FCM objective function for partitioning $\{x_k\}_{k=1}^N$ into c clusters is given by [16]

$$J = \sum_{i=1}^{c}\sum_{k=1}^{N} u_{ik}^p \|x_k - v_i\|^2 \tag{3}$$

where $\{v_i\}_{i=1}^c$ are the prototypes of the clusters and the array $[u_{ik}] = U$ represents a partition matrix, $U \in \mathcal{U}$, namely

$$\mathcal{U}\left\{u_{ik} \in [0, 1] \,\middle|\, \sum_{i=1}^{c} u_{ik} = 1 \;\; \forall\, k \text{ and } 0 < \sum_{k=1}^{N} u_{ik} < N \,\forall\, i\right\}. \tag{4}$$

The parameter p is a weighting exponent on each fuzzy membership and determines the amount of fuzziness of the resulting classification. The FCM objective function is minimized when high membership values are assigned to voxels whose intensities are close to the centroid of its particular class, and low membership values are assigned when the voxel data is far from the centroid [18].

We propose a modification to (3) by introducing a term that allow the labeling of a pixel (voxel) to be influenced by the labels in its immediate neighborhood [21]. As mentioned before, the neighborhood effect acts as a regularizer and biases the solution toward piecewise-homogeneous labeling. Such a regularization is useful in segmenting scans corrupted by salt and pepper noise. The modified objective function is given by

$$J_m = \sum_{i=1}^{c}\sum_{k=1}^{N} u_{ik}^p \|x_k - v_i\|^2 + \frac{\alpha}{N_R}\sum_{i=1}^{c}\sum_{k=1}^{N} u_{ik}^p \left(\sum_{x_r \in \mathcal{N}_k} \|x_r - v_i\|^2\right) \tag{5}$$

where $\mathcal{N}_k$ stands for the set of neighbors that exist in a window around x_k and N_R is the cardinality of $\mathcal{N}_k$. The effect of the neighbors term is controlled by the parameter α. The relative importance of the regularizing term is inversely proportional to the signal-to-noise ratio (SNR) of the MRI signal. Lower SNR would require a higher value of the parameter α.

Substituting (2) into (5), we have

$$J_m = \sum_{i=1}^{c}\sum_{k=1}^{N} u_{ik}^p \|y_k - \beta_k - v_i\|^2 + \frac{\alpha}{N_R}\sum_{i=1}^{c}\sum_{k=1}^{N} u_{ik}^p \left(\sum_{y_r \in \mathcal{N}_k} \|y_r - \beta_r - v_i\|^2\right). \tag{6}$$

Formally, the optimization problem comes in the form

$$\min_{U,\, \{v_i\}_{i=1}^c,\, \{\beta_k\}_{k=1}^N} J_m, \qquad \text{subject to } U \in \mathcal{U}. \tag{7}$$

IV. Parameter Estimation

The objective function J_m can be minimized in a fashion similar to the standard FCM algorithm. Taking the first derivatives of J_m with respect to u_{ik}, v_i, and β_k and setting them to zero results in three necessary but not sufficient conditions for J_m to be at a local extrema. In the following subsections, we will derive these three conditions.

A. Membership Evaluation

The constrained optimization in (7) will be solved using one Lagrange multiplier

$$F_m = \sum_{i=1}^{c}\sum_{k=1}^{N}\left(u_{ik}^p D_{ik} + \frac{\alpha}{N_R}\, u_{ik}^p \gamma_i\right) + \lambda\left(1 - \sum_{i=1}^{c} u_{ik}\right) \quad (8)$$

where $D_{ik} = \|y_k - \beta_k - v_i\|^2$ and $\gamma_i = (\sum_{y_r \in \mathcal{N}_k} \|y_r - \beta_r - v_i\|^2)$. Taking the derivative of F_m with respect to u_{ik} and setting the result to zero, we have, for $p > 1$

$$\left[\frac{\delta F_m}{\delta u_{ik}} = p u_{ik}^{p-1} D_{ik} + \frac{\alpha p}{N_R}\, u_{ik}^p \gamma_i - \lambda\right]_{u_{ik}=u_{ik}^*} = 0. \quad (9)$$

Solving for u_{ik}^* we have

$$u_{ik}^* = \left(\frac{\lambda}{p\left(D_{ik} + \frac{\alpha}{N_R}\gamma_i\right)}\right)^{1/(p-1)}. \quad (10)$$

Since $\sum_{j=1}^{c} u_{jk} = 1 \quad \forall k$

$$\sum_{j=1}^{c}\left(\frac{\lambda}{p\left(D_{jk} + \frac{\alpha}{N_R}\gamma_j\right)}\right)^{1/(p-1)} = 1 \quad (11)$$

or

$$\lambda = \frac{p}{\left(\sum_{j=1}^{c}\left(\frac{1}{\left(D_{jk} + \frac{\alpha}{N_R}\gamma_j\right)}\right)^{1/(p-1)}\right)^{p-1}}. \quad (12)$$

Substituting into (10), the zero-gradient condition for the membership estimator can be rewritten as

$$u_{ik}^* = \frac{1}{\sum_{j=1}^{c}\left(\frac{D_{ik} + \frac{\alpha}{N_R}\gamma_i}{D_{jk} + \frac{\alpha}{N_R}\gamma_j}\right)^{1/(p-1)}}. \quad (13)$$

B. Cluster Prototype Updating

In the following derivation, we use the standard Eucledian distance. Taking the derivative of F_m with respect to v_i and setting the result to zero, we have

$$\left[\sum_{k=1}^{N} u_{ik}^p (y_k - \beta_k - v_i) + \sum_{k=1}^{N} u_{ik}^p \frac{\alpha}{N_R} \sum_{y_r \in \mathcal{N}_k} (y_r - \beta_r - v_i)\right]_{v_i = v_i^*} = 0. \quad (14)$$

Solving for v_i, we have

$$v_i^* = \frac{\sum_{k=1}^{N} u_{ik}^p \left((y_k - \beta_k) + \frac{\alpha}{N_R}\sum_{y_r \in \mathcal{N}_k}(y_r - \beta_r)\right)}{(1+\alpha)\sum_{k=1}^{N} u_{ik}^p}. \quad (15)$$

C. Bias-Field Estimation

In a similar fashion, taking the derivative of F_m with respect to β_k and setting the result to zero we have

$$\left[\sum_{i=1}^{c}\frac{\partial}{\partial \beta_k}\sum_{k=1}^{N} u_{ik}^p (y_k - \beta_k - v_i)^2\right]_{\beta_k = \beta_k^*} = 0. \quad (16)$$

Since only the kth term in the second summation depends on β_k, we have

$$\left[\sum_{i=1}^{c}\frac{\partial}{\partial \beta_k}\, u_{ik}^p (y_k - \beta_k - v_i)^2\right]_{\beta_k = \beta_k^*} = 0. \quad (17)$$

Differentiating the distance expression, we obtain

$$\left[y_k \sum_{i=1}^{c} u_{ik}^p - \beta_k \sum_{i=1}^{c} u_{ik}^p - \sum_{i=1}^{c} u_{ik}^p v_i\right]_{\beta_k = \beta_k^*} = 0. \quad (18)$$

Thus, the zero-gradient condition for the bias-field estimator is expressed as

$$\beta_k^* = y_k - \frac{\sum_{i=1}^{c} u_{ik}^p v_i}{\sum_{i=1}^{c} u_{ik}^p}. \quad (19)$$

D. BCFCM Algorithm

The BCFCM algorithm for correcting the bias field and segmenting the image into different clusters can be summarized in the following steps.

Step 1) Select initial class prototypes $\{v_i\}_{i=1}^{c}$. Set $\{\beta_k\}_{k=1}^{N}$ to equal and very small values (e.g., 0.01).
Step 2) Update the partition matrix using (13).
Step 3) The prototypes of the clusters are obtained in the form of weighted averages of the patterns using (15).
Step 4) Estimate the bias term using (19).

Repeat Steps 2)–4) till termination. The termination criterion is as follows:

$$\|\mathbf{V}_{\text{new}} - \mathbf{V}_{\text{old}}\| < \epsilon \quad (20)$$

where $\|\cdot\|$ is the Euclidean norm, $\mathbf{V}$ is a vector of cluster centers, and ϵ is a small number that can be set by the user.

V. Results and Discussions

In this section, we describe the application of the BCFCM segmentation on synthetic images corrupted with multiplicative gain, as well as digital MR phantoms [28] and real brain MR images. The MR phantoms simulated the appearance and image characteristics of the T1-weighted images. There are many advantages for using digital phantoms rather than real image

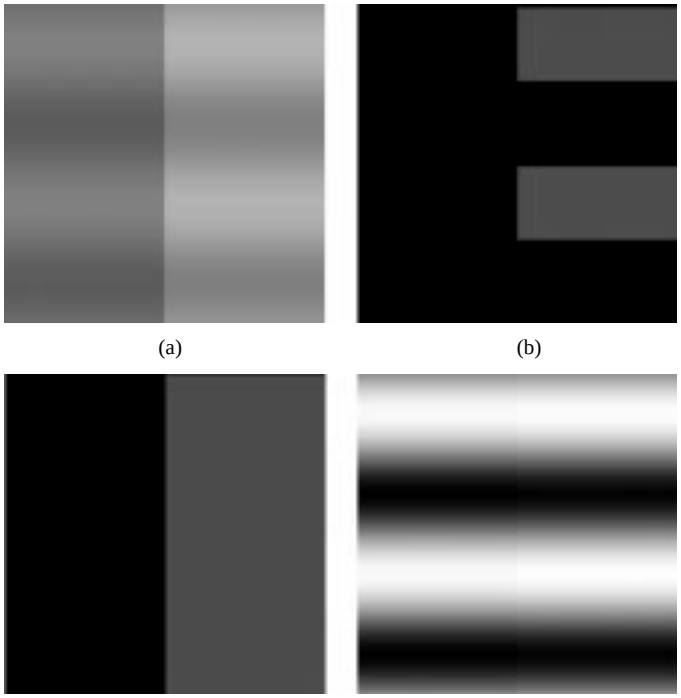

(a) (b) (c) (d)

Fig. 1. Comparison of segmentation results on a synthetic image corrupted by a sinusoidal bias field. (a) The original image. (b) FCM results. (c) BCFCM and EM results. (d) Bias-field estimations using BCFCM and EM algorithms: this was obtained by scaling the bias-field values from one to 255.

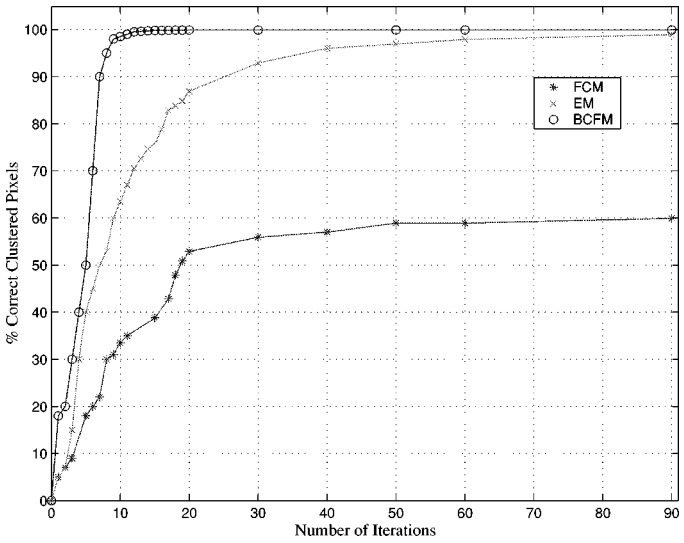

Fig. 2. Comparison of the performance of the proposed BCFCM algorithm with EM and FCM segmentation when applied to the synthetic two-class image shown in Fig. 1(a).

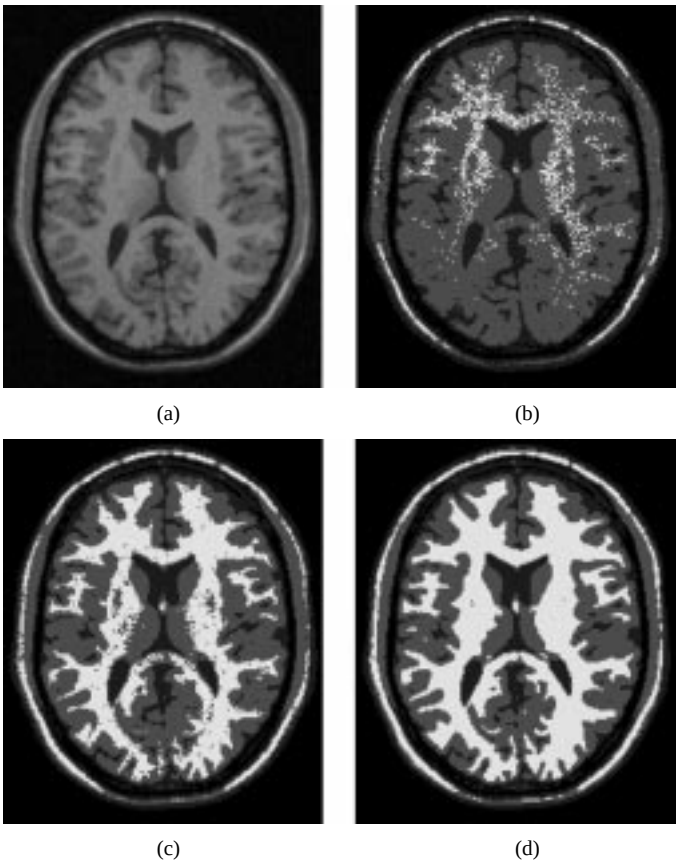

(a) (b) (c) (d)

Fig. 3. Comparison of segmentation results on an MR phantom corrupted with 5% Gaussian noise and 20% intensity inhomogeneity. (a) Original T1-weighted image, (b) using FCM, (c) using EM, and (d) using the proposed BCFCM.

data for validating segmentation methods. These advantages include prior knowledge of the true tissue types and control over image parameters such as mean intensity values, noise, and intensity inhomogeneities. We used a high-resolution T1-weighted phantom with in-plane resolution $= 0.94$ mm^2, Gaussian noise with $\sigma = 6.0$, and three-dimensional linear shading $= 7\%$ in each direction. All of the real MR images shown in this section were obtained using a General Electric Signa 1.5-Tesla clinical MR imager with the same in-plane resolution as the phantom. In all the examples, we set the parameter α (the neighbors effect) to be 0.7, $p = 2$, $N_R = 9$ (a 3×3 window centered around each pixel), and $\epsilon = 0.01$. For low-SNR images, we set $\alpha = 0.85$. The choice of these parameters seem to give the best results.

Fig. 1(a) shows a synthetic test image. This image contains a two-class pattern corrupted by a sinusoidal gain field of higher spatial frequency. The test image is intended to represent two tissue classes, while the sinusoid represents an intensity inhomogeneity. This image was constructed so that it would be difficult to correct using homomorphic filtering or traditional FCM approaches. As shown in Fig. 1(b), FCM algorithm was unable to separate the two classes, while the BCFCM and EM algorithms have succeeded in correcting and classifying the data as shown in Fig. 1(c). The estimate of the multiplicative gain using either BCFCM or EM is presented in Fig. 1(d). This image was obtained by scaling the values of the bias field from one to 255. Although the BCFCM and EM algorithms produced similar results, BCFCM was faster to converge to the correct classification, as shown in Fig. 2.

Figs. 3 and 4 present a comparison of segmentation results between FCM, EM, and BCFCM, when applied on T1-weighted MR phantom corrupted with intensity inhomogeneity and noise. From these images, we can see that traditional FCM was unable to correctly classify the images. Both BCFCM and EM

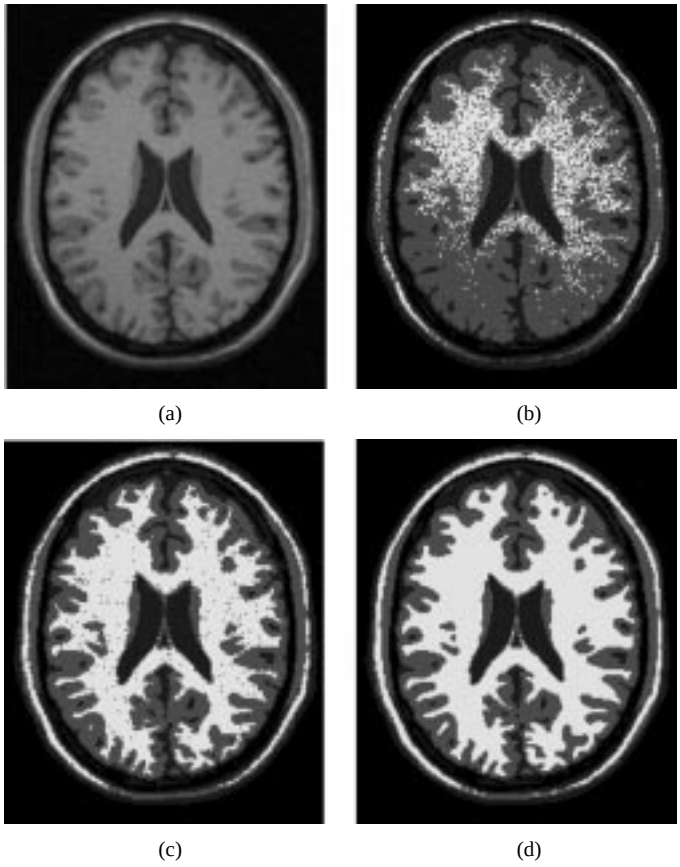

Fig. 4. Comparison of segmentation results on an MR phantom (different slice from Fig. 3) corrupted with 5% Gaussian noise and 20% intensity inhomogeneity. (a) Original T1-weighted image, (b) using FCM, (c) using EM, and (d) using the proposed BCFCM.

segmented the image into three classes corresponding to background, gray matter (GM) and white matter (WM). BCFCM produced slightly better results than EM due to its ability to cope with noise. Moreover, BCFCM requires far less number of iterations to converge compared to the EM algorithm. Table I depicts the segmentation accuracy (SA) of the three mentioned method when applied to the MR phantom. SA was measured as follows:

$$\mathrm{SA} = \frac{\text{Number of correctley classifiedpixels}}{\text{Total number of pixels}} \times 100\%. \tag{21}$$

SA was calculated for different SNR. From the results, we can see that the three methods produced almost similar results for high-SNR. BCFCM method, however, was found more accurate for lower SNR.

Fig. 5 shows the results of applying the BCFCM algorithm to segment a real axial-sectioned T1 MR brain. Strong inhomogeneities are apparent in the image. The BCFCM algorithm segmented the image into three classes corresponding to background, GM and WM. The bottom right image show the estimate of the multiplicative gain, scaled from one to 255.

Fig. 6 shows the results of applying the BCFCM for the segmentation of noisy brain images. The results using traditional FCM without considering the neighborhood field effect and the BCFCM are presented. Notice that the BCFCM segmentation, which uses the neighborhood field effect, is much less fragmented than the traditional FCM approach. As mentioned before, the relative importance of the regularizing term is inversely proportional to the SNR of MRI signal. It is important to notice, however, that the incorporation of spatial constraints into the classification has the disadvantage of blurring of some fine details. There are current efforts to solve this problem by including

TABLE I
SEGMENTATION ACCURACY OF DIFFERENT METHODS WHEN APPLIED ON MR SIMULATED DATA

	SNR		
Segmentation Method	13db	10 db	8db
FCM	98.92	86.24	78.9
EM	99.12	93.53	85.11
BCFCM	99.25	97.3	93.7

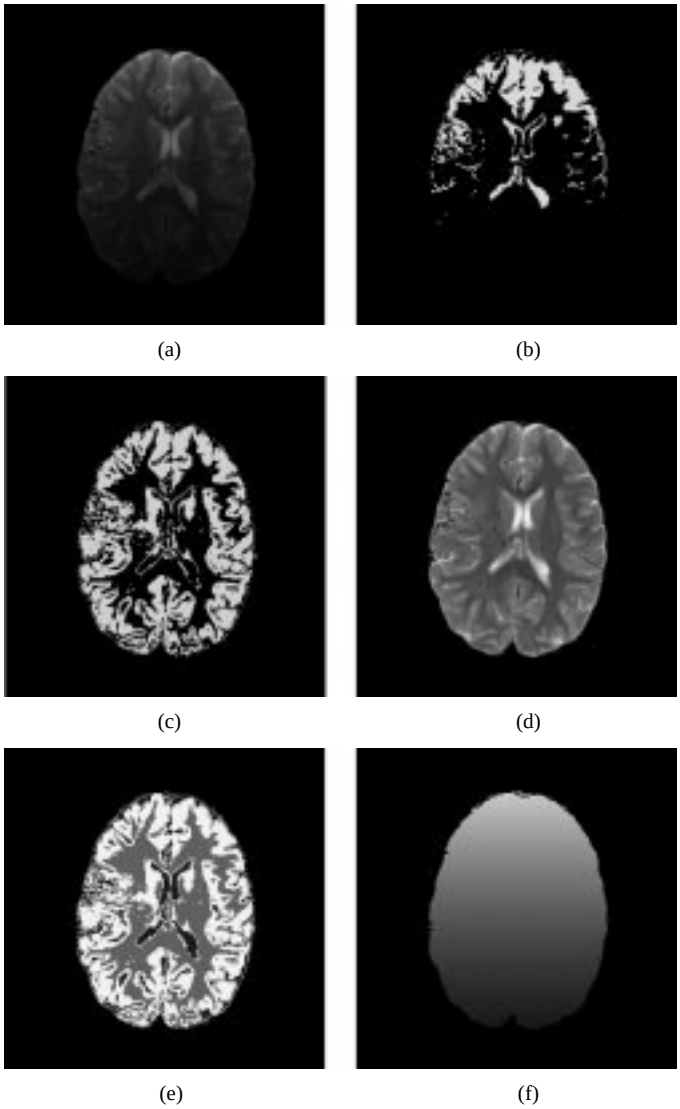

Fig. 5. Brain MRI example. (a) Original MR image corrupted with intensity inhomogeneities. (b) Crisp GM membership using traditional FCM. (c) Crisp GM membership using the proposed BCFCM algorithm. (d) the bias-field corrected image using BCFCM. (e) and (f) Segmented image and bias-field estimate using BCFCM, respectively.

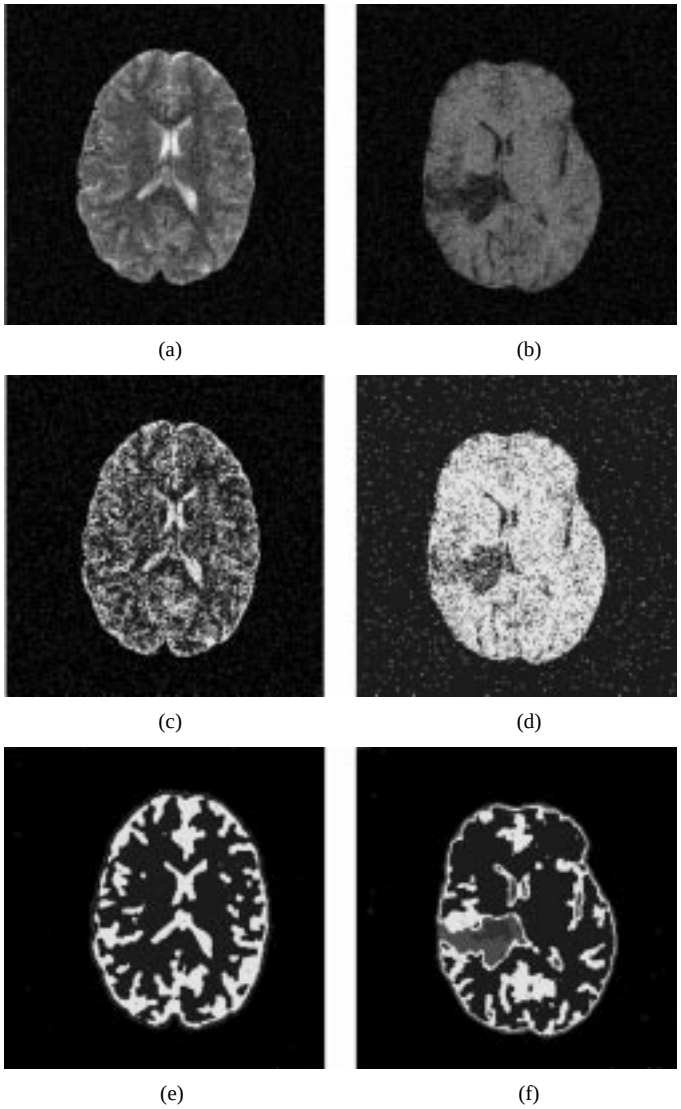

Fig. 6. Brain tumor MRI examples. (a) and (b) Original MR images corrupted with salt and pepper noise, respectively. (c) and (d) Segmented images using FCM without any neighborhood consideration. (e) and (f) Segmented images using BCFCM ($\alpha = 0.85$).

contrast information in the classification. High-contrast pixels, which usually represent boundaries between objects, should not be included in the neighbors.

VI. Conclusion

We have demonstrated a new BCFCM algorithm for adaptive segmentation and intensity correction of MR images. The algorithm was formulated by modifying the objective function of the standard FCM algorithm to compensate for intensity inhomogeneities and to allow the labeling of a pixel (voxel) to be influenced by the labels in its immediate neighborhood. The neighborhood acts as a regularizer and biases the solution toward piecewise-homogeneous labeling; such a regularization is useful in segmenting scans corrupted by salt and pepper noise.

Using simulated MRI data and real brain images reviewed by experts, results show that intensity variations across patients, scans, and equipment changes have been accommodated in the estimated bias field without the need for manual intervention. We compared our results with traditional FCM segmentation and EM algorithm developed by Wells *et al.* [5]. The BCFCM outperformed the FCM on both simulated and real MRI images. The FCM, however, has the advantage of working for vectors of intensities while the BCFCM is limited to single-feature inputs. The BCFCM algorithm produces similar results as the EM algorithm with faster convergence. In noisy images, the BCFCM technique produced better results than the EM algorithm as it compensates for noise by including a regularization term.

The results presented in this paper are preliminary and further clinical evaluation is required. The evaluation of the method for localized measurements, such as the impact on tumor boundary or volume determinations also needs further work, as the current phantom measurements are based on more global corrections for image nonuniformity.

Acknowledgment

The authors would like to thank the reviewers for their valuable comments and suggestions.

References

[1] B. R. Condon, J. Patterson, and D. Wyper, "Image nonuniformity in magnetic resonance imaging: Its magnitude and methods for its correction," *Br. J. Radiol.*, vol. 60, pp. 83–87, 1987.

[2] E. R. McVeigh, M. J. Bronskil, and R. M. Henkelman, "Phase and sensitivity of receiver coils in magnetic resonance imaging," *Med. Phys.*, vol. 13, pp. 806–814, 1986.

[3] D. A. G. Wicks, G. J. Barker, and P. S. Tofts, "Correction of intensity nonuniformity in MR images of any orientation," *Magn. Reson. Imag.*, vol. 11, pp. 183–196, 1993.

[4] A. Simmons, P. S. Tofts, G. J. Barker, and S. R. Arrdige, "Sources of intensity nonuniformity in spin echo images at 1.5T," *Magn. Reson. Med.*, vol. 32, pp. 121–128, 1994.

[5] W. M. Wells, III, W. E. L. Grimson, R. Kikinis, and F. A. Jolesz, "Adaptive segmentation of MRI data," *IEEE Trans. Med. Imag.*, vol. 15, pp. 429–442, Aug. 1996.

[6] B. Johnston, M. S. Atkins, B. Mackiewich, and M. Anderson, "Segmentation of multiple sclerosis lesions in intensity corrected multispectral MRI," *IEEE Trans. Med. Imag.*, vol. 15, pp. 154–169, Apr. 1996.

[7] J. G. Sled, A. P. Zijdenbos, and A. C. Evans, "A nonparametric method for automatic correction of intensity nonuniformity in MRI data," *IEEE Trans. Med. Imag.*, vol. 17, pp. 87–97, Feb. 1998.

[8] S. Lai and M. Fang, "A new variational shape-from-orientation approach to correcting intensity inhomogeneities in MR images," in *Proc. Workshop Biomedical Image Analysis, CVPR98*, Santa Barbara, CA, 1998, pp. 56–63.

[9] C. R. Meyer, P. H. Bland, and J. Pipe, "Retrospective correction of intensity inhomogeneities in MRI," *IEEE Trans. Med. Imag.*, vol. 14, pp. 36–41, Feb. 1995.

[10] M. Tincher, C. R. Meyer, R. Gupta, and D. M. Williams, "Polynomial modeling and reduction of RF body coil spatial inhomogeneity in MRI," *IEEE Trans. Med. Imag.*, vol. 12, pp. 361–365, Apr. 1993.

[11] B. H. Brinkmann, A. Manduca, and R. A. Robb, "Optimized homomorphic unsharp masking for MR grayscale inhomogeneity correction," *IEEE Trans. Med. Imag.*, vol. 17, pp. 161–171, Apr. 1998.

[12] B. Dawant, A. Zijidenbos, and R. Margolin, "Correction of intensity variations in MR images for computer-aided tissue classification," *IEEE Trans. Med. Imag.*, vol. 12, pp. 770–781, Dec. 1993.

[13] S. Gilles, M. Brady, J. Declerck, J. P. Thirion, and N. Ayache, "Bias field correction of breast MR images," in *Proc. 4th Int. Conf. Visualization in Biomedical Computing*, Hamburg, Germany, Sept. 1996, pp. 153–158.

[14] C. Brechbuhler, G. Gerig, and G. Szekely, "Compensation of spatial inhomogeneity in MRI based on a parametric bias estimate," in *Proc. 4th Int. Conf. Visualization in Biomedical Computing*, Hamburg, Germany, Sept. 1996, p. 141 and 146.

[15] R. Guillemaud and M. Brady, "Estimating the bias field of MR images," *IEEE Trans. Med. Imag.*, vol. 16, pp. 238–251, June 1997.

[16] J. C. Bezdek and S. K. Pal, *Fuzzy Models for Pattern Recognition*. Piscataway, NJ: IEEE Press, 1991.

[17] J. C. Dunn, "A fuzzy relative of the ISODATA process and its use in detecting compact well-separated clusters," *J. Cybern.*, vol. 3, pp. 32–57, 1973.
[18] J. Bezdek, "A convergence theorem for the fuzzy ISODATA clustering algorithms," *IEEE Trans. Pattern Anal. Machine Intell.*, vol. PAMI-2, pp. 1–8, 1980.
[19] C. Xu, D. Pham, and J. Prince, "Finding the brain cortex using fuzzy segmentation, isosurfaces, and deformable surfaces," in *Proc. XVth Int. Conf. Information Processing in Medical Imaging (IPMI 97)*, 1997, pp. 399–404.
[20] D. L. Pham and J. L. Prince, "Adaptive fuzzy segmentation of magnetic resonance images," *IEEE Trans. Med. Imag.*, vol. 18, pp. 737–752, Sept. 1999.
[21] M. N. Ahmed, S. M. Yamany, N. A. Mohamed, A. A. Farag, and T. Moriarty, "Bias field estimation and adaptive segmentation of MRI data using modified fuzzy C-means algorithm," in *Proc. IEEE Int. Conf. Computer Vision and Pattern Recogn.*, vol. 1, Fort Collins, CO, June 1999, pp. 250–255.
[22] J. K. Udupa and S. Samarasekera, "Fuzzy connectedness and object definition: Theory, algorithm and applications in image segmentation," *Graphical Models Image Processing*, vol. 58, no. 3, pp. 246–261, 1996.
[23] S. M. Yamany, A. A. Farag, and S. Hsu, " A fuzzy hyperspectral classifier for automatic target recognition (ATR) systems," *Pattern Recogn. Lett.*, vol. 20, pp. 1431–1438, 1999.
[24] J. Bezdek, L. Hall, and L. Clarke, "Review of MR image segmentation using pattern recognition," *Med. Phys.*, vol. 20, pp. 1033–1948, 1993.
[25] M. E. Brandt, T. P. Bohan, L. A. Kramer, and J. M. Fletcher, "Estimation of CSF, white matter and gray matter volumes in hydrocephalic children using fuzzy clustering of MR images," *Comput. Med. Imag. Graph.*, vol. 18, pp. 25–34, 1994.
[26] L. O. Hall, A. M. Bensaid, L. P. Clarke, R. P. Velthuizen, M. S. Silbiger, and J. C. Bezdek, "A comparison of neural network and fuzzy clustering techniques in segmenting magnetic resonance images of the brain," *IEEE Trans. Neural Networks*, vol. 3, pp. 672–682, Sept. 1992.
[27] N. A. Mohamed, "Modified fuzzy C-mean algorithm for medical image segmentation," M.Sc. thesis, Elect. Eng. Dept., Univ. Louisville, Louisville, KY, 1999.
[28] A. F. Goldszal, C. Davatzikos, D. L. Pham, M. X. H. Yan, R. N. Bryan, and S. M. Resnick, "An image processing system for qualitative and quantitative volumetric analysis of brain images," *J. Comput. Assist. Tomogr.*, vol. 22, no. 5, pp. 827–837, 1998.